LEM
WORKING PAPER SERIES

A multiscale network-based model of contagion dynamics: heterogeneity, spatial distancing and vaccination

Maíra Aguiar [a,b,c]
Giovanni Dosi [d]
Damián A. Knopoff [a,e,f]
Maria Enrica Virgillito [d]

[a] Basque Center for Applied Mathematics (BCAM), Bilbao, Spain.
[b] Dipartimento di Matematica, Università degli Studi di Trento, Italy.
[c] Ikerbasque, Basque Foundation for Science, Bilbao, Spain.
[d] Institute of Economics and EMbeDS, Scuola Superiore Sant'Anna, Pisa, Italy.
[e] Centro de Investigación y Estudios de Matemática (CIEM - CONICET), Córdoba, Argentina.
[f] FaMAF, Universidad Nacional de Córdoba, Argentina.

A multiscale network-based model of contagion dynamics: heterogeneity, spatial distancing and vaccination

Maíra Aguiar[1], Giovanni Dosi[2], Damián A. Knopoff[3] and Maria Enrica Virgillito[4]

[1] Basque Center for Applied Mathematics (BCAM), Mazarredo, 14, 48009, Bilbao, Spain; Dipartimento di Matematica, Università degli Studi di Trento, Italy; Ikerbasque, Basque Foundation for Science, Bilbao, Spain; maguiar@bcamath.org

[2] Institute of Economics and EMbeDS, Scuola Superiore Sant'Anna, Piazza Martiri della Liberta' 33, 56127, Pisa, Italy, gdosi@santannapisa.it

[3] Basque Center for Applied Mathematics (BCAM), Mazarredo, 14, 48009, Bilbao, Spain; Centro de Investigación y Estudios de Matemática (CIEM - CONICET), Córdoba, Argentina; FaMAF, Universidad Nacional de Córdoba, Medina Allende s/n, 5000, Córdoba, Argentina, dknopoff@bcamath.org

[4] Institute of Economics and EMbeDS, Scuola Superiore Sant'Anna, Piazza Martiri della Liberta' 33, 56127, Pisa, Italy, mariaenrica.virgillito@santannapisa.it (Corresponding author)

June 29, 2021

Abstract

Lockdown and vaccination policies have been the major concern in the last year in order to contain the SARS-CoV-2 infection during the COVID-19 pandemic. In this paper we present a model able to evaluate alternative lockdown policies and vaccination strategies. Our approach integrates and refines the multiscale model proposed by Bellomo *et al.*, 2020, analyzing alternative network structures and bridging two perspectives to study complexity of living systems. Inside different matrices of contacts we explore the impact of closures of distinct nodes upon the overall contagion dynamics. Social distancing is shown to be more effective when targeting the reduction of contacts among and inside the most vulnerable nodes, namely hospitals/nursing homes. Moreover, our results suggest that school closures alone would not significantly affect the infection dynamics and the number of deaths in the population. Finally, we investigate a scenario with immunization in order to understand the effectiveness of targeted vaccination policies towards the most vulnerable individuals. Our model agrees with the current proposed vaccination strategy prioritising the most vulnerable segment of the population to reduce deaths.

Keywords: pandemic; COVID-19; epidemiological models; kinetic theory; active particles; spatial patterns; networks; vaccination; health policies
AMS Subject Classification: 92C60, 92D30

1 Introduction

Although the use of SIR type models has been widely adopted by policy makers [1, 2, 3] in order to obtain predictions about COVID-19 spreading, a severe respiratory syndrome caused by a new coronavirus (SARS-CoV-2), many limitations have been acknowledged to this simple modelling approach, particularly regarding the role of heterogeneity, which has been shown to significantly affect disease transmission and control. Although the influence of age affecting death probability in a population is often assumed, only few modeling frameworks are currently able to include heterogeneity via social networks structures, see e.g., [23, 25, 28].

In this paper, using a multiscale network-based model of contagion dynamics, we explore the role of heterogeneity in shaping and unfolding the overall diffusion process of COVID-19 epidemic. An extensive simulation analysis considering different social network structures is performed to investigate the impact of social interactions during the pandemic. Results are compared addressing the effectiveness of social distancing policies. The impact of an immunization strategy is also investigated to understand the effectiveness of the current COVID-19 vaccination protocols prioritising the most vulnerable individuals.

The model is able to account for two forms of heterogeneity, namely between-individual heterogeneity in virus transmission on the basis of individual attributes influencing the epidemic growth, and social-structure heterogeneity, introducing alternative forms of networks influencing the contact dynamics as well as different structured nodes within which contacts occur, namely schools, hospitals/nursing homes, workplaces and households. In so doing, we explicitly model the two crucial factors affecting the reproduction number of the epidemic, hence the most sought information by policy-makers during COVID-19 crisis, contagion, i.e., between-individual virus transmission, and contact, i.e, the social structure interaction of individuals in a population.

Methodologically, we make a bridge between two different approaches to model complex behaviour in living systems. The first approach is the kinetic theory of active particles (KTAP thereafter) [11] which allows to model macroscopic states as the result of multi-level interactions occurring at microscopic states, going from the relationship between the virus and the immunological system (within-host dynamics) toward the population dynamics (between-host dynamics). The KTAP approach has been successfully employed to innovatively model the contagion dynamics of the COVID-19 spreading [10, 12]. The second approach is the complex system analysis of social networks which has seen in the last decades an increasing number of studies documenting the network properties of social relationships, quite far away from homogenous distributions, and in general characterised by repeated, structured and clustered contacts [33]. Both approaches share the view of biological and social organizations as complex systems, often evolving, and indeed provide many common interpretations of real world phenomena.

Simulation-based results of the developed model support the role played by network structure in affecting the social distancing policies implemented during the pandemic. In particular, comparing random, scale-free and small-world graphs, we study the dynamics of contacts occurring among the four different types of nodes above mentioned, each of them characterized by different size, immunity of the pop-

ulation and probability of contacts with other nodes. The dynamics of the epidemic is studied with reference to crucial parameters influencing the network structure and connectivity, mainly the wiring probability and the degree (number of contacts).

Inside alternative contact matrices we study the impact of closures of different nodes upon the overall contagion dynamics. As we shall show, social distancing is more effective when targeting the reduction of contacts among and within the most vulnerable nodes, namely hospitals/nursing homes. On the other hand, school closures do not appear to be the most effective policy measure, not affecting significantly the reduction of deaths in the population. Finally, we experiment with a set-up on immunization in order to understand the effectiveness of targeted vaccination policies towards the most vulnerable individuals. According to our model, vaccinating first the most vulnerable segment of the population has an important role to reduce deaths in the population.

The paper is structured as follows. Section 2 discusses the two modelling approaches integrated in this paper. Section 3 presents the model and its dynamics, and Section 4 presents simulation results on social distancing and vaccinations. The last section concludes this work.

2   KTAP and complex networks

The kinetic theory of active particles [9] represents a powerful avenue to formalize processes of contagion and progression of infections. This approach shares with the classical kinetic theory [13] the representation of a large system of interacting entities by a probability distribution function over their individual state, e.g., at the microscopic scale. The dynamics is obtained by equating the time derivative of the probability distribution to the difference between the inlet and the outlet flux in an elementary volume of the space of the microscopic states.

Refs. [5, 11] present an overview of the applications and covered domains in which the KTAP has been employed, ranging from socio-economic systems [4, 17] to models of mutating virus [16] and bacterial antibiotic resistance [27]. Unlike the standard kinetic theory [13], the microscopic state is not only identified by the position and velocity of the particles, but it also includes a vector of additional variables, called *activity*, which models the forms of interactions. The whole system can be subdivided into groups of interest called *functional subsystems*, in short, FSs. Additionally, interactions, which in the classical kinetic theory are governed by basic principles of classical mechanics, in the *active particles* (in short *a-particles*) approach are modelled by stochastic interactions, wherein actors/agents are identified by probability distributions. In so doing, interactions do not simply involve individual entities but also collections of them.

Irreversibility of the interaction processes and potential state-dependent parameters fuel the non-linear nature of the approach, increasing the level of complexity and calling for a computational analysis. Indeed, diverse types of behaviors of agents and more generally system complexity [6] might be appropriately modelled.

In the following, inspired by [9], our mathematical derivation will avoid mean-field approximations to let extreme behaviors emerge. Complementary but different approaches closer to a kinetic theory allowing for Boltzmann and Fokker-Plank equations are in [20, 32], while mathematical tools of statistical-stochastic dynamics are

in [22].

The sequential steps of the derivation of the model include:

(1) Representation of the functional subsystems involved in the dynamics, where FSs are constituted by active particles, and where each FS expresses one or more functions defined as activities.

(2) Derivation of a mathematical structure suitable to describe the dynamics of the dependent variables derived in the first step.

(3) Specification of individual interactions by inserting them into the general mathematical structure derived in the second step.

From the KTAP approach to complex networks, the extensive review in [33] discusses the advances made in integrating classic mathematical models of epidemic spreading (SIR or SIS types) with complex networks.

As acknowledged by the authors such research path gave origin to a long series of results and modelling techniques quite scattered among different disciplines. In summary, the integration of epidemic models with network structures has been systematized in three different approaches.

Individual-based mean-field (IBMF) whose basic idea is to build evolution equations for the probability of a given individual (node) to belong to a given compartment, assuming independence from the state of each node with respect to its own neighbourhood. The method is akin to mean-field theory assuming factorization between probabilities and it has been mainly used to find solutions in static networks.

To study the evolution of dynamical processes on networks it has been employed the Degree-based mean-field (DBMF) which instead of working at the individual level, it assumes that all nodes of the same degree are statistically equivalent, therefore variables are specified at the degree and not at the individual level. The approach deals with the probability that a given individual with a given node degree belongs to a given compartment. In this case, the adjacency matrix is not expressed in terms of individual contacts, but rather in terms of average contacts among nodes of different degrees. The approach is used to describe processes of epidemic diffusion occurring at a lower time scale than interaction dynamics, as in this case, the network, although maintaining its distribution is always rewired.

The third approach is the Generating function which is used to describe a problem of percolation inside a network. In this case the link between two nodes depends on the probability of transmission of the disease from one infectious node to a susceptible one. It therefore nests contagion and contact in the same probability.

Although advancing with respect to homogenous SIS/SIR models, such types of modelling attempts mainly make heterogeneous the transition probability of belonging to each of the compartment, or alternatively link the creation of the network structure with the propagation of the virus.

Compared to the extant modelling approaches, the following model presents many different characteristics:

- The model completely detaches the process of virus propagation from the structure of interactions among individuals.

4

- The propagation of infection is based on entity-level differential equations which define endogenous transition probabilities different across entities.

- The dynamics of contagion is then nested into the dynamics of complex networks, which dynamically evolve.

- The model entails alternative micro-meso-macro levels of interactions:

  - within-host (virus vs antibodies),

  - between-individual (different functional subsystems),

  - within-node, whereby nodes represent different structures/places, and not individuals,

  - between-node, whereby each node is linked to neighbours on the basis of the underlying network structure,

  - population level dynamics in terms of overall number of infected, recovered, susceptible, deceased cases.

Given that the characterization of each node is not in terms of single individuals but rather in terms of populations/places, and considering that each node is populated by individuals (particles) which can move connecting two nodes of the network, our model is more akin to a particle-network metapopulation approach. This framework considers that particles inside each given node may react according to specific mechanisms, while across nodes diffuse creating edges depending on the attributes of the nodes, mainly degree. This representation makes the whole system of epidemic spreading similar to a reaction-diffusion model. When applied to SIR, it has been shown that metapopulation models present threshold points in determining the outbreak of the epidemic, also labelled invasion threshold depending on the mobility between nodes [38].

3   The mathematical model

Let us consider a population of spatially homogeneous distributed individuals. Each individual can belong, at each time t, to one of the following compartments or FSs: susceptible (S-FS), infected (I-FS), recovered (R-FS) or deceased (D-FS). The S-FS is assumed to have only an outlet flow (into the I-FS), while R-FS and D-FS have only an inlet flow (from I-FS), i.e., we assume that recovered individuals get a long lasting immunity and remain in that compartment, as schematized in Fig. 1.

The micro-state of every individual is described by a variable $w \in [0, 1]$ corresponding to the level of activation of the immune defence. It is convenient to discretize into a set

$$\mathbf{w} = \{w_1 = 0, \ldots, w_k = \frac{k-1}{n-1}, \ldots, w_n = 1\},$$

such that n risk groups (e.g., according to age or presence of co-morbidities) are considered. In this way, $w_1 = 0$ and $w_n = 1$ correspond, respectively, to the lowest and highest immune system activation.
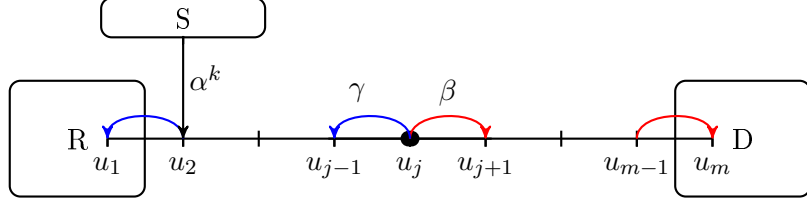
Figure 1: Susceptible individuals can get infected with an infection rate α^k, entering to the infected compartment with state u_2. Then, competitive interactions between the virus that proliferates with rate β towards more aggressive states and the immune system which acts with rate γ may end up with a transition into the R or D compartments.

In addition, within the I-FS individuals are also characterized by a variable $u \in [0,1]$ representing the level of progression of the viral infection (e.g., from mild to severe). If m possible states are considered, we have

$$\mathbf{u} = \{u_1 = 0, \ldots, u_p = \frac{p-1}{m-1}, \ldots, u_m = 1\}.$$

Here, if an individual reaches the state $u_1 = 0$ we assume that it is recovered from the infection (transition into R), while reaching the state $u_m = 1$ implies a decease (transition into D).

The representation of the system is given by the following distribution functions:

- $f_S^k(t)$ is the probability to find, at time t, a susceptible individual with micro-state w_k. Susceptible population at time t, $f_S(t)$, is simply computed by the zero-th order moment $\sum_{k=1}^{n} f_S^k(t)$.

- $f_I^{p,k}(t)$ is the probability to find, at time t, an infected individual with micro-state (u_p, w_k). Prevalence at time t is given by $f_I(t) = \sum_{k=1}^{n} \sum_{p=2}^{m-1} f_I^{p,k}(t)$.

- $f_R^k(t)$ is the probability to find, at time t, a recovered individual with micro-state w_k. The cumulative recovered population, $f_R(t)$, is simply computed by the sum $\sum_{k=1}^{n} f_R^k(t)$.

- $f_D^k(t)$ is the probability to find, at time t, a deceased individual with micro-state w_k. As for the recovered, the cumulative deceased population $f_D(t)$ is given by $\sum_{k=1}^{n} f_D^k(t)$.

The system of equations representing the evolution of the distribution functions,

whose derivation can be followed in details in [10], is given by

$$
\begin{cases}
\dfrac{d}{dt} f_S^k(t) = -\sum_{l=1}^{n} \sum_{q=2}^{m-1} \alpha^k\, u_q\, f_S^k(t)\, f_I^{q,l}(t), \\[2ex]
\dfrac{d}{dt} f_I^{p,k}(t) = \sum_{l=1}^{n} \sum_{q=2}^{m-1} \alpha^k\, u_p\, f_S^k(t)\, f_I^{q,l}(t)\, \delta_{2p} + \beta u_{p-1}\, f_I^{p-1,k}(t) \\[1ex]
\qquad\qquad + \gamma\, w_k\, f_I^{p+1,k}(t) - \beta\, u_p\, f_I^{p,k}(t) - \gamma\, w_k\, f_I^{p,k}(t), \\[2ex]
\dfrac{d}{dt} f_R(t) = \gamma \sum_{k=1}^{n} w_k\, f_I^{2,k}(t), \\[2ex]
\dfrac{d}{dt} f_D(t) = \beta\, u_{m-1} \sum_{k=1}^{n} f_I^{m-1,k}(t),
\end{cases}
\tag{1}
$$

where for $(1)_1$ one has $k = 1, \ldots, n$, while for $(1)_2$ one has $p = 2, \ldots, m-1$ and $k = 1, \ldots, n$. Equation $(1)_1$ describes the infection of susceptible individuals due to interactions with infected ones. Equation $(1)_2$ describes the dynamics within the infected population. The factor δ_{2p} denotes a Kronecker delta function, meaning that the entry state immediately upon infection is u_2, and from that state a competitive interaction between viral particles and the immune system begins, as illustrated in Fig. 1. Then, Eqs. $(1)_3$ and $(1)_4$ give the inlet flows into recovered and deceased classes, respectively, as a result of the afore mentioned competitive interactions. Regarding model parameters, α^k is the infection rate of individuals with micro-state w_k, β is the viral progression rate and γ the immune action rate towards recovery.

3.1   Network structure

Let us now consider that the dynamics described above takes place within several nodes of an undirected weighted network $\mathcal{G} = (V, E)$, where V is a set of N nodes and E is a set of edges joining some pairs of nodes. Let $A = [a_{ij}]_{i,j=1\ldots,N}$ be the adjacency matrix of $\mathcal{G}$, such that its elements indicate whether pairs of vertices are linked or not. The entries of the adjacency matrix are equal to zero if there is no edge linking nodes i and j, while they are positive if i and j are linked through an edge. The existence of a link between two nodes implies that the epidemic may spread with positive probability from one to the other. We make the following assumptions:

- Entries $a_{ij} \in [0, 1]$ weigh the "intensity" of the interaction between nodes i and j.

- Within each node there is a subpopulation of individuals belonging to one of the classes S, I, R or D.

- To keep the model as a generalization of the one presented above, there is an edge connecting each node to itself, namely a self-loop. Let $a_{ii} = 1$ for $i = 1, \ldots, N$.

- The network is undirected. Consequently, A is symmetric.

7

Let f_{iS}^k, $f_{iI}^{p,k}$, f_{iR} and f_{iD} denote the distribution functions of susceptible, infected, recovered and deceased individuals within node i, for $i = 1, \ldots, N$, $k = 1, \ldots, n$ and $p = 1, \ldots, m$. The system (1) can be now formulated for the entire network as follows:

$$
\begin{cases}
\dfrac{d}{dt} f_{iS}^k(t) = -\sum_{j=1}^N \sum_{l=1}^n \sum_{q=2}^{m-1} a_{ij}\, \alpha_i^k\, u_q\, f_{iS}^k(t)\, f_{jI}^{q,l}(t), \\[3mm]
\dfrac{d}{dt} f_{iI}^{p,k}(t) = \sum_{j=1}^N \sum_{l=1}^n \sum_{q=2}^{m-1} a_{ij}\, \alpha_i^k\, u_p\, f_{iS}^k(t)\, f_{jI}^{p,l}(t)\, \delta_{2p} + \beta u_{p-1}\, f_{iI}^{p-1,k}(t) \\[3mm]
\qquad + \gamma\, w_k\, f_{iI}^{p+1,k}(t) - \beta\, u_p\, f_{iI}^{p,k}(t) - \gamma\, w_k\, f_{iI}^{p,k}(t), \\[3mm]
\dfrac{d}{dt} f_{iR}(t) = \gamma \sum_{k=1}^n w_k\, f_{iI}^{2,k}(t), \\[3mm]
\dfrac{d}{dt} f_{iD}(t) = \beta\, u_{m-1} \sum_{k=1}^n f_{iI}^{m-1,k}(t),
\end{cases}
\tag{2}
$$

where α_i^k is the contagion rate of individuals with state w_k within node i.

Model parameters and variables are summarized in Table 1 to bear in mind the notation.

Parameter	Meaning
n	Number of immune states
$I_w = \{w_1, \ldots, w_k, \ldots w_l, \ldots, w_n\}$	Immune states
m	Number of states of viral progression
$I_u = \{u_1, \ldots, u_p, \ldots u_q, \ldots, u_m\}$	Viral progression states
N	Network size
$A = [a_{ij}]$	Adjacency matrix
α_i^k	Infection rate for individuals with state w_k within node i
β	Disease progression rate
γ	Immune action rate

Table 1: Model parametrization.

3.2 Within node dynamics

In order to characterize each node as a distinct metapopulation, we consider four classes of nodes which are distinguished in terms of three attributes, namely, size (number of individuals inside each node), distribution of immunity which is a proxy for age and presence of other co-morbidities, multiplicity of each class of node. To sum up, we include in the model:

Node type	Node population	Immune distribution	Color code
Household	5	Centered	Green
School	150	Skewed-right	Blue
Hospital	150	Skewed-left	Red
Company	150	Centered	Black

Table 2: Parametrization of each node type.

- Household: this node is the most copious, each of them populated by few individuals, whose immunity is distributed according to a symmetric distribution, with far from the average values quite unlikely. Being families characterised by individuals of different ages, their immunity distribution is expected to be well-mixed.

- School: this node is characterised by a higher number of individuals compared to households and presents a right-skewed immune distribution,

  with higher values more probable than lower ones, in line with the empirical evidence according to which infection rates are lower among younger people.

- Hospital/nursing home: this node is characterised by a higher number of individuals compared to households and presents a left-skewed immune distribution, with lower values more probable than higher ones, in line with the empirical evidence according to which infection rates are higher among elderly or patients already exposed to other co-morbidities. Therefore, the higher infection rate emerging out of a left-skewed immune distribution might reflect either an older population (nursing homes) or the presence of individuals with other co-morbidities (hospitals).[1]

- Company: this node is characterised by a higher number of individuals compared to households and presents a symmetric immune distribution with far from the average values quite unlikely. Being companies characterised by individuals of different ages, but generically of ages comprised in the range 20 - 65 years, their immunity distribution is expected to be well-mixed as families.

In order to avoid mixing different attributes at the same time, we parametrize immunity equally distributed in households and companies; additionally we set the same size in terms of number of individuals for companies, hospitals and schools. The final parametrization is presented in Table 2.

Figure 2 shows the immune distribution of the population within each of the different node types as well as the dynamics of cumulative infected, recovered and deceased cases, assuming in all cases 1 initial infected individual. A common feature across all four nodes is the emergence of an outburst in the period 50-100, with however different shapes across nodes with schools converging at a much slower rate, less concave when compared to the rest.

---

[1]In the remaining of the paper we will exclusively refer to hospital for the sake of simplicity.

A strong heterogeneity emerges when looking at different within-node dynamics. With reference to nodes of the same size but different in immunity distribution, the latter clearly influences not only the speed of diffusion, but also the overall fraction of infected and deceased cases, ranging from almost the total in hospitals to one third in schools in case of infected, and from two to fifty deaths from schools to hospitals. When comparing nodes of different size but with the same immunity distribution, households and companies present the same fraction of deceased cases (one tenth), while the number of individuals in each cluster only influences the speed of diffusion, without altering the shape.

The within-node dynamics is governed by the interaction rate parameter α_i^k which has been on purpose kept equal across all nodes, therefore heterogeneity mainly derives from different immunity distributions.

3.3   Network dynamics

Once defined the dynamics in each node, we open the structure of interrelationship allowing for contacts across different populations, each located inside a different node and now having the chance to move reaching another node.

In order to characterize the structure of interactions, we start with the easiest network topology, considering zero clustering and a Poisson distribution of contacts, namely the Erdös-Rényi graph which assumes that contacts occur with a completely random order.

A random network consists of N nodes where each node pair is connected with wiring probability p. Each node is statistically equivalent to another. Such a network can be constructed as follows [7, 21]:

1. Start with N isolated nodes.

2. Select a node pair and generate a random number between 0 and 1. If the number exceeds p, connect the selected node pair with a link, otherwise leave them disconnected.

3. Repeat the previous step for each of the $N(N-1)/2$ pairs of nodes.

Figure 3 illustrates a random network obtained with $N = 20$ nodes and wiring probability $p = 0.15$. Each node belongs to one of the categories introduced above, namely household (green), school (blue), hospital (red) and company (black). In this case, a category was randomly assigned to each node in such a way that 15 of them are households, while the other 5 are distributed among the other categories.

Dynamics for a single realization of the experiment with $N = 200$ is shown in Figures 4 and 5, where low and high wiring probabilities are considered. Most of the nodes are assumed to be households, with a lower number of schools, hospitals and companies, as may be the case e.g., of a neighbourhood. A first result is that under a low wiring probability (cf. Figure 4), connecting the previously isolated nodes, instead of making the outbreak exploding actually reduces the spreading with respect to the case of isolated nodes. Notably, the number of infected individuals is quite low and no outburst of the epidemic occurs. The result is in line with the literature documenting that introducing some forms of heterogeneity in the structure of contacts reduces the outbreak [36]. However, when looking at a very high wiring

probability (cf. Figure 5) a different dynamics emerges with a large cumulative fraction of infected and deceased cases.

Figure 6 shows the final epidemic size and cumulative deaths for many realizations of the random network with different wiring probabilities. A strong threshold effect in the dynamics of the epidemic is visible: in order to have an actual outburst the wiring probability needs to reach 50% meaning that any two individuals of different nodes have a probability to meet in one case over two. Threshold effects are quite expected in such type of modelling approach and there exist two limit cases: if $p = 0$ the epidemic will remain confined in each of the population nodes, without diffusing. Under $p \to 1$ the epidemic will spread across all-over the nodes because all individuals visit each node with certainty. In our case $p \in [0.4, 0.5]$ defines the transition point, or global invasion threshold at which the epidemic spreads [33]. A strong correlation indeed emerges between increasing wiring probabilities and fraction of infected/deceased cases, corroborating the role played by the topological structure of the network.

In order to experiment with the role played by the latter network structure, we now construct a Watts-Strogatz diffusion process to link the nodes. Such network is a random graph with small-world graph properties, such as clustering and short average path length [40]. A small world network with N nodes is constructed in the following way [30]:

1. Create a ring lattice with N nodes of mean degree $2K$. Each node is connected to its K nearest neighbours.

2. For each edge in the graph, with independent and uniform probability $\tilde{p}$, that edge is removed and replaced by a new edge between two nodes that are chosen uniformly at random from the N nodes, without duplicating or self-looping edges.

In this way, when $\tilde{p} = 0$, a ring graph in which each node is coupled to its K nearest neighbours is obtained. On the other hand, when $\tilde{p} = 1$, the result is a random graph [34]. The topology of a small-world network is illustrated in Figure 7 for $N = 20$, $K = 2$ and two different wiring probabilities.

Finally, we experiment with large connectivity of few hubs and low connectivity of the majority of nodes, as represented by the case of scale-free networks. The following algorithm produces a Barabási-Albert undirected scale-free network of size N. It begins with an initial network of size m_0 and then $N - m_0$ nodes are introduced sequentially into the network, where each node connects with $m^* \leq m_0$ existing nodes. Note that it is typical to choose $m_0 = m^*$. One cannot choose $m^* > m_0$ as then the first new node introduced cannot be assigned m^* edges. Thus, the initial network size m_0 determines the maximum mean degree of the network. The m^* existing nodes are chosen with a probability which is proportional to their current degree; the combination of network growth with this preferential attachment is what leads to a power-law degree distribution [8]. We have adapted the algorithm by [39] based on [35]. The topology of a scale-free network is illustrated in Figure 8 for $N = 20$, $m_0 = 3$ and two different preferential attachment values m.

Comparing different network structures in Fig. 9, showing an ER, a WS small world and a scale-free BA graphs, we do not observe any systematic difference in the

overall dynamics, as far as the three graphs are parametrized in "comparable" way. This suggests that the dynamics and eventual outbreak of the disease depend on the network connectivity. Therefore in Figure 10 we show the final size of cumulative infected (here we kept only the figures for infected cases in order to have a better resolution, since deceased show the same dynamics) as a function of three alternative measures of centrality, namely mean degree, mean closeness and mean betweenness for an ensemble of realizations of the model with the three graphs.

For each graph, centrality of a node represents how much the node of interest is influential in spreading the virus. Centrality might be measured by the mean degree which defines the probability that a randomly chosen vertex has degree k, mean closeness which defines how much a node is close to another on average in terms of shortest paths, mean betweenness which defines the average importance of a node with respect to others in terms of connections it captures as shortest paths, that is the amount of information the node controls. The experiment, which is run under randomly chosen parameters (differently from the one presented in Fig. 9 which confronts comparable parametrizations) reveals that:

- Threshold (phase-transition) behaviours are present independently of the graph under study and occur in the proximity of similar values of mean degree, closeness and betweenness.

- Degree and closeness centralities positively correlate with the outspread after a given threshold is reached, independently from the graph under study: the higher the number of edges for each node or the closeness between two nodes, the higher the possibility of the outburst, but only after a given threshold parameter. On the other side, below a certain threshold, reducing the number of links or making them more distant is irrelevant in affecting the shape of the epidemic.

- Betweenness centrality negatively correlates with the outspread after a given threshold is reached independently from the graph under study. Notice that the betweenness of a node is calculated as the proportion of shortest paths in the network that pass through it. Nodes with large betweenness centrality value often act as bridges between distant clusters but have small degrees. Thus, networks with large mean betweenness resemble one dimensional grids, explaining the negative correlation with the outspread.

4   Social distancing and vaccination

Taking as a departure point the random network with the same features as in Fig. 5, some experiments are now conducted in order to analyse different ways of reducing contacts. Given the structure of our model, social distancing might be performed under alternative strategies: i) reducing between-node contacts, ii) reducing within-node contacts, iii) reducing both within- and between-node contacts, iv) comparing reduction of contacts among alternative nodes, v) targeting specific nodes.

4.1 Between-node contacts reduction

We start by experimenting with the strategy of between-node contacts reduction.[2] Fig. 11 shows the effect of reducing the weights of the edges connecting alternative nodes. While a_{ii} is kept equal to 1 for all $i = 1, \ldots, N$, a_{ij} $(i \neq j)$ now takes different weights from 0.6 to 1 from a given "locking time", supposed to be at $T_{lock} = 100$. The reduction of weights from 1 to 0.6 effectively reduces the spreading of the epidemic with substantial impacts in terms of cumulative infected and deceased cases, almost halved when reducing the between-node propagation. It is worth mentioning that the entries of the adjacency matrix are changed in such a way that it preserves the symmetry.

We now move to analyse which type of between-node contacts reduction is more effective, recalling that they are differentiated in terms of immunity and size. Figure 12 shows, respectively, the scenario in which only schools (first row), only hospitals (second row) or only companies (third row) are closed (100% closure) or partially closed (50% closure), while the rest of nodes keep receiving flows of individuals.

Comparing contacts reduction in terms of alternative nodes, school closures appear to be the less effective in terms of reducing the number of cumulative infected and deceased cases: particularly in terms of deaths we observe that a reduction of the weights of connections toward schools from 1 to 0 marginally affects the total number of deceased cases in the system. At the opposite, the reduction of weights connecting hospitals from 1 to 0 strongly affects the number of deaths, while company closures represent an intermediate case, for sure more effective than school closures in containing the epidemic. Recall that the three nodes are differentiated only in terms of the immunity distribution, while the size and the numerousness among them is comparable. Therefore, the latter heterogeneous effects are only due to the within-host dynamics affected by different immunity distributions.

Figure 13 compares one by one node closures under the three alternative network configurations in order to study the robustness of our results and to detect the extent to which different connectivity might play a role. In all three studied networks, school closures are the less effective social distancing strategy particularly in affecting the number of deaths.

4.2 Between-node vs within-node contacts reduction

The next experiment consists in comparing the effects of reducing between-node contacts vs reducing the intensity of interactions inside each node. The experiment allows to understand the extent to which it is more effective mitigating the spreading of the contagion inside each node or conversely the diffusion across nodes. The trade-off is not trivial since lockdown policies restricting the access to different nodes are socially more strenuous than controlling interactions inside each node.

Results are presented in Figure 14 where we compare three alternative scenarios under a common random graph. At time $t = 100$ the lockdown might consist in:

---

[2]In the following, we exclude contacts reduction from and toward households since, given the symmetric property of the adjacency matrix, it will entail the unreasonable scenario of preventing individuals to reach their home. Note also that households have the same qualitative dynamics of companies, being characterised by the same immune distribution (cf. Figure 2.)

a. reducing social interactions within each node via the parameter α_i^k;

b. reducing the diffusion across nodes via weights in the adjacency matrix;

c. reducing the number of edges that connect nodes.

In all three cases the reduction is set at 25%. Acknowledging that strategy [c] is the most invasive for society since it implies the deterministic deletion of some edges, in our case identified randomly but potentially identifiable also on the basis of node centrality (so called hubs), strategy [b] results indeed to be less effective than [a] in mitigating the overall diffusion. In fact, reduction of interactions inside nodes not only mitigates the peak of infection but also delays it.

Having considered alternative ways to undertake lockdown measures and their effectiveness, we now present the scenario in which the lockdown strategy is considered to be the most effective. We label this experiment as "protecting the vulnerable" and we introduce a set-up in which we compare reduction of social interactions for the vulnerable segment of the population, denoted by α_i^1, and reducing weights of edges connecting to hospitals (cf. Figure 15). In both cases the reduction was done at 50%. While the first experiment is directed in controlling virus diffusion among the most vulnerable segment, the elderly or people affected by co-morbidities, the second experiment allows to reduce the access to hospitals/nursing homes to avoid the possibility of spreading the infection in such places. From the model results, coupling the two strategies would be the most effective policy in mitigating the number of deaths.

4.3   Vaccination

The final experiment we conduct consists in analysing the impact of vaccination targeting a given population. Defining the target population from which starting the vaccination is a complex task from a health management point of view and there have been different possibilities on how to do it. In [14] two alternative strategies have been discussed, assuming that vaccines are able to protect against disease and infection, either i) the immunization of the most vulnerable segment of the population or ii) the immunization of super-spreaders.[3]

Although the existing COVID-19 vaccines are reported with remarkable effectiveness against severe disease, the sterilizing immunity conferred by these vaccines are still being evaluated. Our model considers an imperfect vaccine with vaccinated individuals able to transmit the disease even when a certain level of immunity is acquired. Here, our baseline assumption is that immunizing primarily the vulnerable individuals would reduce deaths, whereas immunizing primarily the so called "super-spreaders" would contain the diffusion of the disease.

According to our model, virus transmission does not only depend on the number and structure of contacts, as the super-spreader strategy would entail, but also on the biological evolution of the virus. The within-host dynamics is equally if not more important than the structure of contacts in determining the transmission: most vulnerable individuals not only have higher chances to get infected but also of

---

[3]Super-spreaders represent the 20% fraction of the population responsible for 80% of infections, according to the 80-20 Pareto law of cumulative processes [14].

die out of the infection. Additionally, this fraction is not only more vulnerable but also more contagious because of high viral loads concentrating in elderly residency and hospitals.

In order to test the effectiveness of targeted vaccination toward the most vulnerable segment of the population, we define an experiment according to which:

- We employ the ER random network with $N = 200$ and $p = 0.9$ as a sample graph (see Fig. 5).

- Each realization of the experiment consists in choosing randomly a proportion of the total nodes, and within the chosen nodes we "vaccinate the vulnerable individuals". We model the effect of vaccination "moving" those individuals with states w_1 and w_2 to the highest level w_n.

After 200 realizations of the experiment, we get the results shown in Fig. 16. The Spearman correlation coefficient is around -0.9. The reduction in terms of infected and deceased cases strongly increases with the number of vaccinated nodes just immunizing a small fraction of the population inside each node. The number of vaccinated people for each realization depends on the randomly chosen nodes and can be computed by looking at how many individuals belong to the classes w_1 and w_2 for each node type (see left panel in Fig. 2). Note that nodes have not been targeted in this experiment but chosen randomly. We fit by means of a Least Squares (SLQ) robust filter the scattered points obtained under repeated MC realizations: a deterministic sigmoidal filter well approximates the dynamics signalling that the variance across realizations does not explode.

Even in this random set-up, which does not start from e.g., hospitals/nursing homes, protecting the vulnerable contributes significantly in reducing the burden of the epidemics in terms of deaths.

5   Conclusions

Lockdown and vaccination policies have been the major concern in the last year in order to contain the SARS-CoV-2 transmission. We present a model able to study the impact of different lockdown policies and vaccination strategies. It integrates and refines the multiscale approach presented in [10] by means of alternative network structures, therefore bridging two perspectives to study complexity of living systems [11]. While the multiscale approach allows to tackle both the within- and between-host dynamics, modelling the problem of virus propagation as a competition process between immunity and the virus itself, contacts among individuals are structured within nodes via a constant probability, and across nodes via network dynamics. Additionally, we characterize four alternative nodes in terms of their size and immunity distributions, namely households, companies, schools and hospitals/nursing homes. Methodologically, our model can be seen as a metapopulation multiscale model able to interact biological and social dynamics.

Simulation results have shown that protecting the vulnerable hub, namely hospitals/nursing homes, by reducing their contact with the other hubs and contacts within the hub would influence significantly the reduction of deaths, whereas reduction of contacts toward the most heterogeneous hubs, namely schools and companies,

would not affect the number of decease cases as much, but rather influencing on disease transmission. Clearly, controlling the diffusion of the virus <u>inside</u> nodes is very important and effective in containing the epidemics.

Moreover, the within-host dynamics allows to implement vaccine administration and to evaluate the impact of different strategies, which we are able to study acting on the immunity distribution of individuals. We show that protecting the most vulnerable segment of the population is very effective in reducing deaths and eventually transmission.

Lockdowns are carriers of an enormous mental stress at the societal level and therefore must be limited and properly planned to be effective. They have inequality enhancing effects, impinging more on children and youth, women, and migrants. In terms of social side-effects, lockdowns have to be assessed in light of i) the low effect they have when put in place generically, without targeting specific segments of the population (nodes in our modelling set-up), ii) the challenge they represent for early stage education because of school closures, hardly substitutable via online schooling for the majority of pupils [24, 31, 37]. In terms of economic side-effects, lockdowns enormously exacerbate disparities among those who can telework, maintaining income and job security, versus those who cannot, at risk of unemployment and income losses [15]. In the last year, workplace safety, particularly in segments like logistic and food processing, has been largely missing and this calls again for the implementation of targeted policies at workplaces well beyond lockdowns [19].

Studies like the one described here are of major importance to understand the dynamical behaviour of epidemics in a population. As an example, our model allows to study the role played by workplaces as hubs of virus spreading and have showed that mitigating accesses to companies is indeed more effective than reducing accesses to schools. Moreover, our model also shows that prioritizing vaccination towards the most vulnerable is the most effective strategy to reduce severe cases and deaths.

From a global health-management perspective, although after six months many rich countries got decent immunization rates, the majority of developing countries still misses vaccines. Under vaccine scarcity, immunizing the most vulnerable segments in less-developed areas of the globe should be the priority. Therefore, plans to make vaccine production free and easily replicable, relaxing intellectual property rights and promoting transfer of know how should be encouraged by international institutions, starting with the World Trade Organization. Related, international agreements favouring the acquisitions of vaccines from non-producing countries at controlled prices should be fostered as well [18].

Among many potential modelling refinements, the direct extension would entail the inclusion of an economic process regulating the relationship among companies in order to study the coupled dynamics between the biological system, the social structure of interactions and economic outcomes.

Acknowledgements

References

[1] M. Aguiar , J. Bidaurrazaga Van-Dierdonck, J. Mar, N. Cusimano, D. Knopoff, V. Anam and Nico Stollenwerk, Critical fluctuations in epidemic models explain COVID-19 post-lockdown dynamics, *Nature Sci. Rep.*, to appear (2021).

[2] M. Aguiar, J. Bidaurrazaga Van-Dierdonck and N. Stollenwerk, Reproduction ratio and growth rates: measures for an unfolding pandemic, *PLoS ONE*, **15** (2020) e0236620 (14 pages).

[3] M. Aguiar, E. Millán Ortuondo, J. Bidaurrazaga Van-Dierdonck, J. Mar and N. Stollenwek, Modelling COVID 19 in the Basque Country from introduction to control measure response, *Nature Sci. Rep.*, **10** (2020) 17306.

[4] G. Ajmone Marsan, N. Bellomo and M. Egidi, Towards a mathematical theory of complex socio-economical systems by functional subsystems representation, *Kinet. Relat. Mod.*, **1** (2008) 249–278.

[5] G. Ajmone Marsan, N. Bellomo and L. Gibelli, Stochastic evolutionary differential games toward a systems theory of behavioral social dynamics, *Math. Models Methods Appl. Sci.*, **26** (2016) 1051–1093.

[6] P. Ball, Why Society is a Complex Matter (Springer-Verlag, 2012).

[7] A. Barabasi, Network Science (Cambridge University Press, 2016).

[8] A. L. Barabasi and R. Albert, Emergence of scaling in random networks, *Science*, **286** (1999) 509–512.

[9] N. Bellomo, A. Bellouquid, L. Gibelli and N. Outada, A Quest Towards a Mathematical Theory of Living Systems (Birkhäuser, New York, 2017).

[10] N. Bellomo, R. Bingham, M. A. J. Chaplain, G. Dosi, G. Forni, D. A. Knopoff, J. Lowengrub, R. Twarock and M. E. Virgillito, A multi-scale model of virus pandemic: Heterogeneous interactive entities in a globally connected world, *Math. Models Methods Appl. Sci.*, **30** (2020) 1591–1651.

[11] N. Bellomo, D. Burini, G. Dosi, L. Gibelli, D. Knopoff, N. Outada, P. Terna and M.E. Virgillito, What is life? A perspective of the mathematical kinetic theory of active particles, *Math. Models Methods Appl. Sci.*, to appear (2021).

[12] N. Bellomo, D. Burini,N. Outada, Multiscale models of COVID-19 with mutations and variants, *Netw. Heterog. Media*, to appear (2021).

[13] C. Cercignani, R. Illner and M. Pulvirenti, The Mathematical Theory of Diluted Gas (Springer-Heidelberg, New York, 1993).

[14] C. Cox, The Vulnerable Can Wait. Vaccinate the Super-Spreaders First, in: https://www.wired.com/story/covid-19-vaccine-super-spreaders/. Retrieved June 14, 2021.

[15] A. Cetrulo, D. Guarascio, M.E. Virgillito, The privilege of working from home at the time of social distancing, *Intereconomics*, **55** (2020) 142-147.

[16] S. De Lillo, M. Delitala and M. Salvatori, Modelling epidemics and virus mutations by methods of the mathematical kinetic theory for active particles, *Math. Models Methods Appl. Sci.*, **19** (2009) 1405–1425.

[17] M. Dolfin, D. Knopoff, L. Leonida and D. Patti, Escaping the trap of "blocking": a kinetic model linking economic development and political competition, *Kinet. Relat. Mod.*, **10** (2017) 423–443.

[18] G. Dosi, Some policy lessons from medical/therapeutic responses to the COVID- 19 Crisis: A rich research system for knowledge generation and dysfunctional institutions for its exploitation, *Intereconomics*, to appear (2021).

[19] EFAT, Covid-19 outbreaks in slaughterhouses and meat processing plants, in: https://effat.org/wp-content/uploads/2020/09/ Covid-19-outbreaks-in-slaughterhouses-and-meat-processing-plants-State-of-affairs-and- 09.2020.pdf. Retrieved June 14, 2021.

[20] G. Furioli, A. Pulvirenti, E. Terraneo and G. Toscani, Fokker-Planck equations in the modeling of socio-economic phenomena, *Math. Models Methods Appl. Sci.*, **27** (2017) 115–158.

[21] E. N. Gilbert, Random graphs, *Ann. Math. Stat.*, **30** (1959) 1141–1144.

[22] D. Helbing, Quantitative Sociodynamics. Stochastic Methods and Models of Social Interaction Processes (Springer Berlin Heidelberg, 2nd edition, 2010).

[23] H. A. Herrmann and J. M. Schwartz, Why COVID-19 models should incorporate the network of social interactions, *Phys. Biol.*, **17** (2020) 065008.

[24] M. M. Jæger and E. H. Blaabæk, Inequality in learning opportunities during Covid-19: Evidence from library takeout, *Res. Soc. Strat. Mobil.*, **68** (2020) 100524–100524.

[25] M.J. Keeling and K.T.D Eames , Networks and epidemic models, *J. R. Soc. Interface*, **2** (2005) 295–307.

[26] M. J. Keeling, , *Proc. R. Soc. B*, **2666** (1999) 859.

[27] D. Knopoff and J.M. Sánchez, A kinetic model for horizontal transfer and bacterial antibiotic resistance, *Int. J. Biomath.*, **10** (2019) 1750051 (21 pages).

[28] G. Manzo, Complex Social Networks are Missing in the Dominant COVID-19 Epidemic Models, *Sociologica*, **14** (2020) 31–49.

[29] J. C. Miller, , *Phys. Rev. E*, **80** (2009) 020901.

[30] MathWorks, (2015). Build Watts-Strogatz Small World Graph Model. Retrieved June 14, 2021 from https://es.mathworks.com/help/matlab/math/build-watts-strogatz-small-world-graph-model.html

[31] E.S. McBryde, J.M. Trauer, A. Adekunle, R. Ragonnet and M.T. Meehan, Stepping out of lockdown should start with school re-openings while maintaining distancing measures. Insights from mixing matrices and mathematical models, medRxiv 2020.05.12.20099036; doi: https://doi.org/10.1101/2020.05.12.20099036

[32] L. Pareschi and G. Toscani, Interacting Multiagent Systems: Kinetic Equations and Monte Carlo Methods (Oxford University Press, Oxford, 2013).

[33] R. Pastor-Satorras, C. Castellano, P. V. Mieghem and A. Vespignani, Epidemic processes in complex networks, *Rev. Mod. Phys.*, **87** (2015) 925–979.

[34] M.A. Porter, Small-world network, *Scholarpedia*, **7(2)** (2012) 1739.

[35] B. J. Prettejohn, M. J. Berryman and M. D. McDonnell. Methods for generating complex networks with selected structural properties for simulations: a review and tutorial for neuroscientists, *Front. Comput. Neurosci.*, **5** (2011) 11.

[36] H. Rahmandad, J.Sterman, Heterogeneity and Network Structure in the Dynamics of Diffusion, *Management Science*, **54** 998-1014, **1**, 249-278, 2008.

[37] G. Rozhnova, C.H. van Dorp, P. Bruijning-Verhagen, et al. Model-based evaluation of school- and non-school-related measures to control the COVID-19 pandemic, *Nat. Commun.*, **12** (2021) 1614.

[38] N. Stollenwerk and V. Jansen, Population Biology and Criticality (Imperial College Press, London, 2011).

[39] Tapan (2021). Scale free network using B-A algorithm

(https://www.mathworks.com/matlabcentral/fileexchange/49356-scale-free-network-using-b-a-algorithm), MATLAB Central File Exchange. Retrieved June 14, 2021.

[40] D.J. Watts and S.H. Strogatz, Collective dynamics of "small-world" networks, *Nature*, **393(1)** (1998) 440–442.
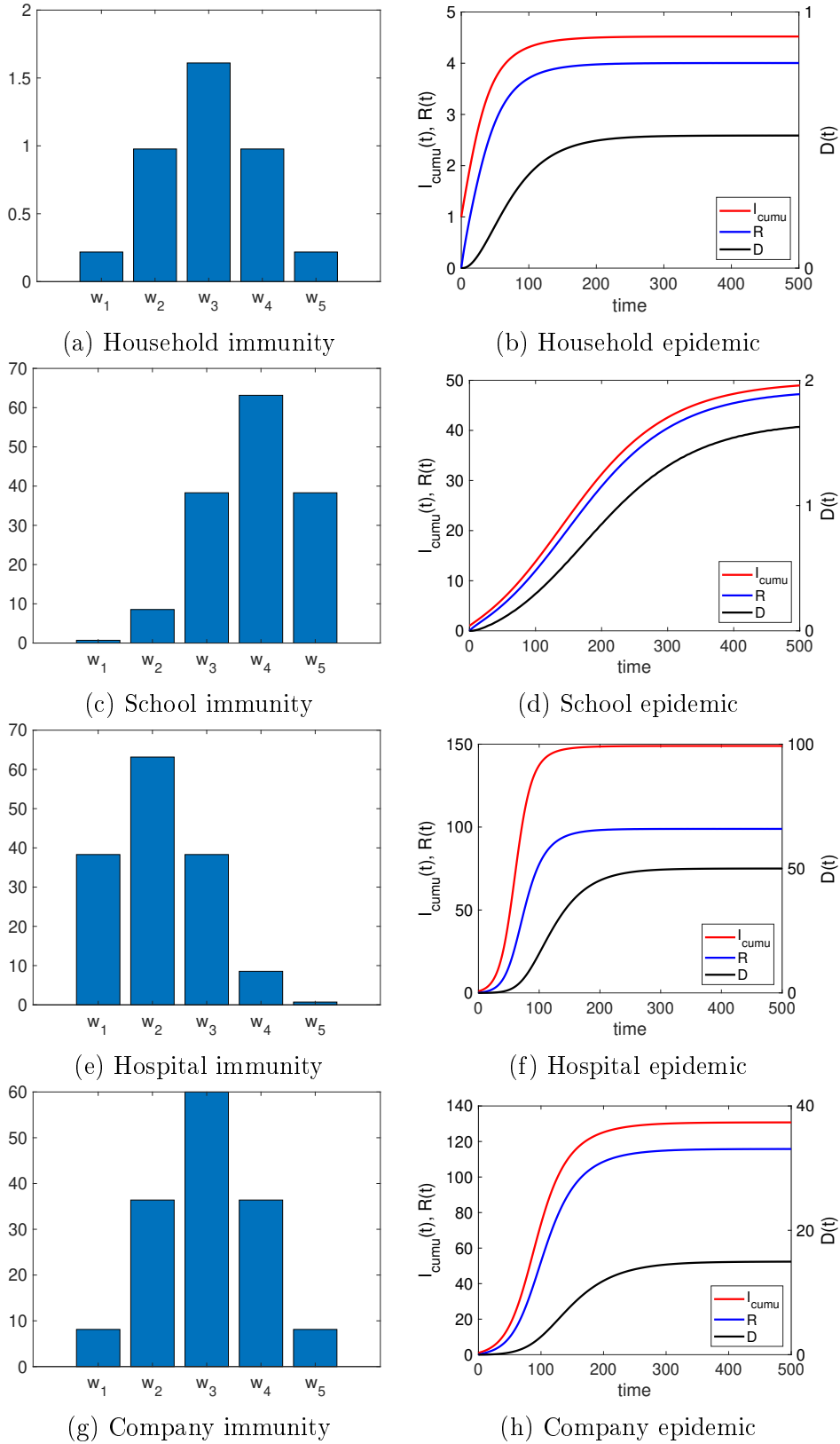
Figure 2: Frequency distribution of immunity levels w_k (left panel) for each node type, and cumulative infected, recovered and deaths (right panel) assuming initially one infected individual in the node.

20
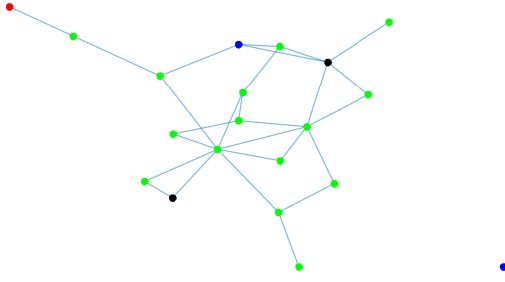
Figure 3: Random network with $N = 20$ and $p = 0.15$. The color node code is: green = household; blue = school; red = hospital; black = company.
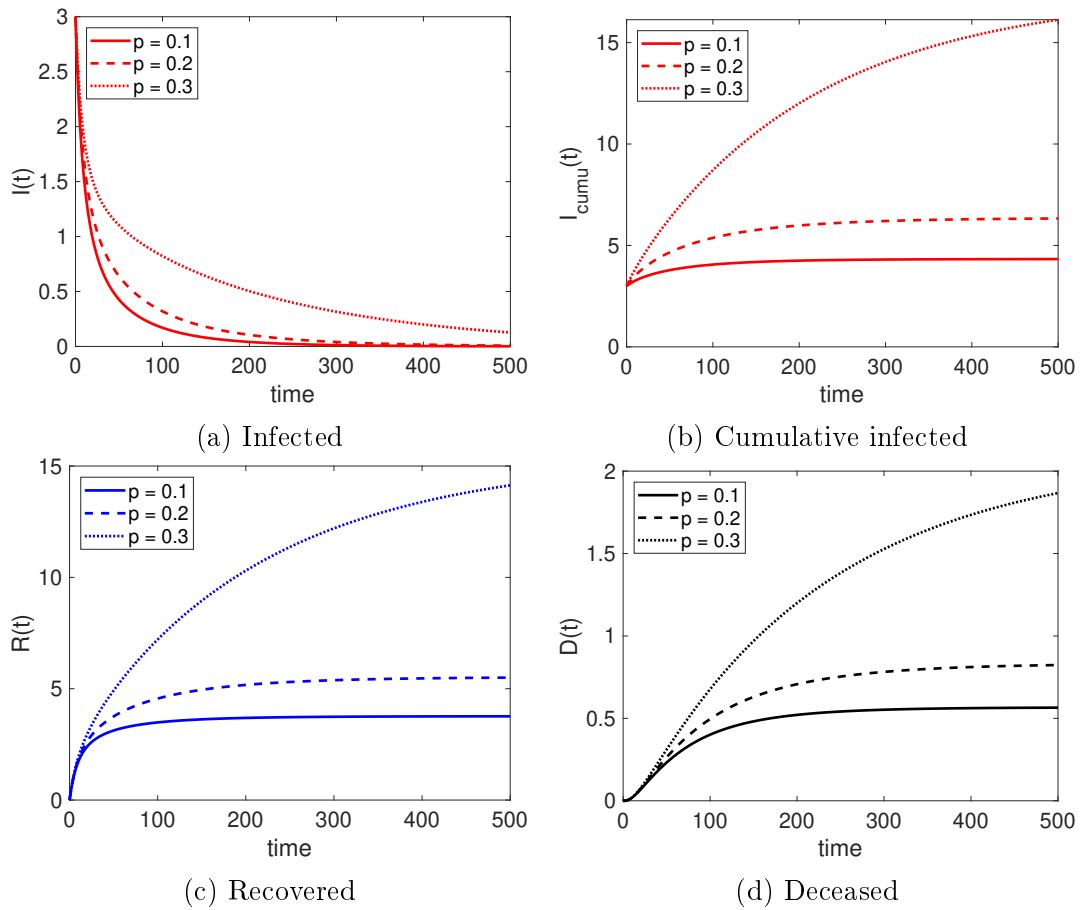

(a) Infected

(b) Cumulative infected

(c) Recovered

(d) Deceased

Figure 4: Random network with $N = 200$ and $p = 0.1, 0.2, 0.3$, with 195 households, 2 schools, 1 hospital and 2 companies. The total population is 1725 with 5 initial infected individuals. Parameter values are $\alpha_i^k = 0.4$, $\beta = 0.1$ and $\gamma = 0.2$. Curves represent (a) prevalence $I(t)$, (b) cumulative infected $I_{cumu}(t)$, (c) recovered $R(t)$ and (d) deceased $D(t)$.

21
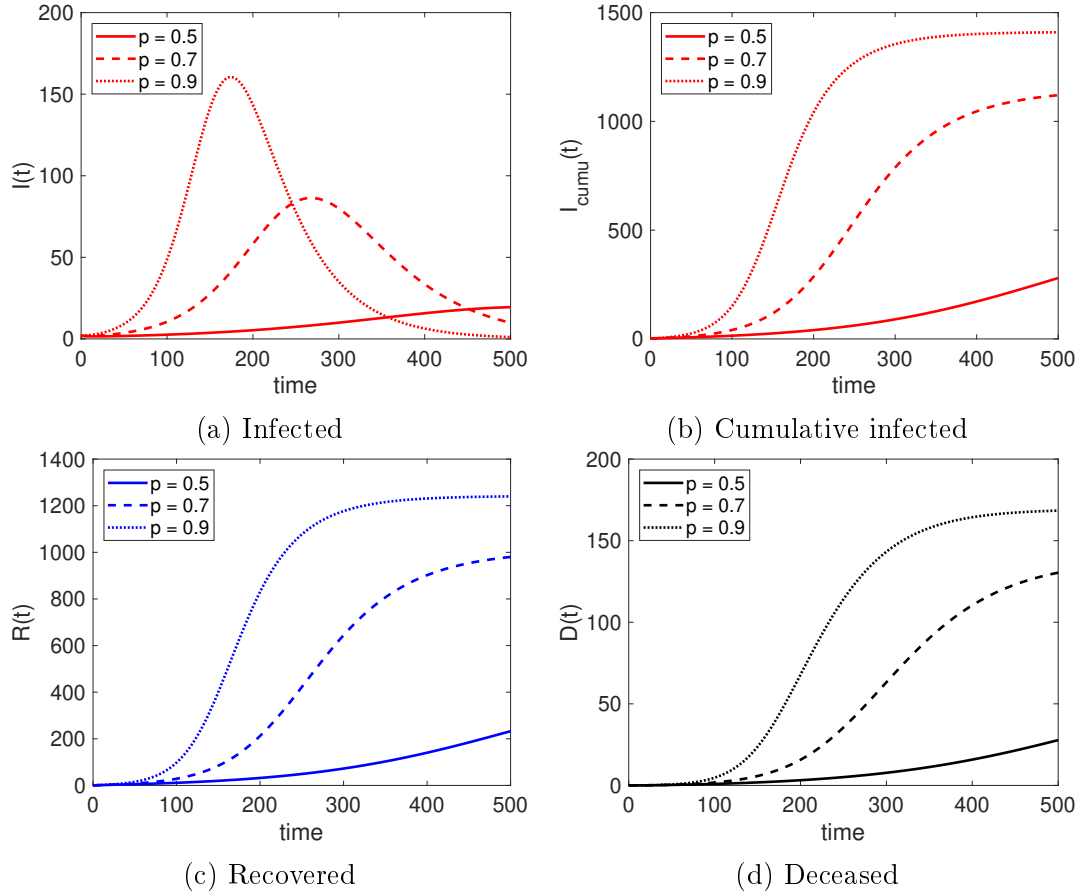
Figure 5: Random network with $N = 200$ and $p = 0.5, 0.7, 0.9$, with 195 households, 2 schools, 1 hospital and 2 companies. The total population is 1725 with 5 initial infected individuals. Parameter values are $\alpha_i^k = 0.4$, $\beta = 0.1$ and $\gamma = 0.2$. Curves represent (a) prevalence $I(t)$, (b) cumulative infected $I_{cumu}(t)$, (c) recovered $R(t)$ and (d) deceased $D(t)$.
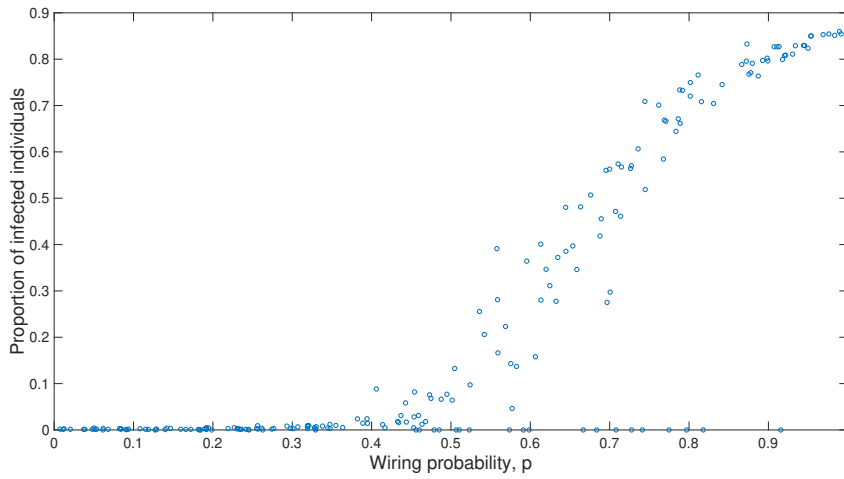
(a) Final epidemic size vs wiring probability
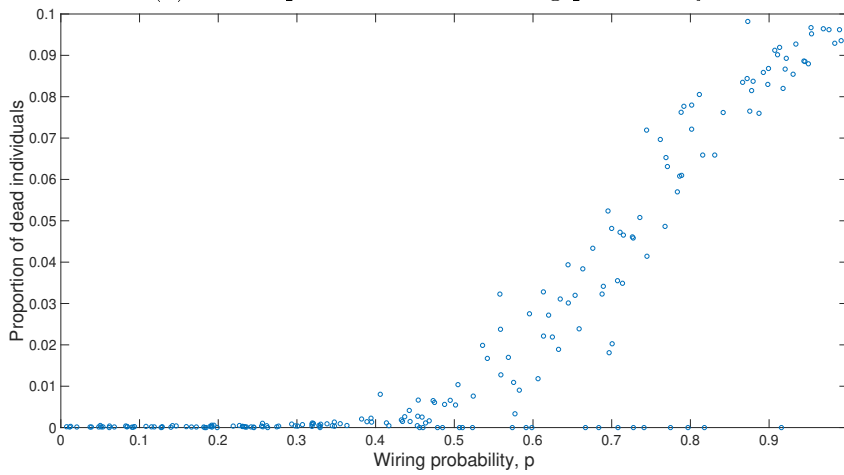
(b) Cumulative deaths vs. wiring probability

Figure 6: (a) Final epidemic size and (b) cumulative deaths vs. wiring probability, for 200 realizations of the random network. Spearman correlation coefficient of 0.75.
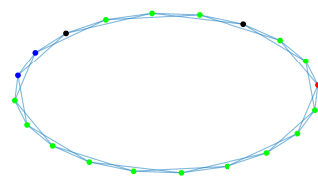
(a) $\tilde{p} = 0$
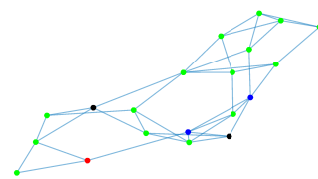
(b) $\tilde{p} = 0.1$

Figure 7: Watts-Strogatz small world network with $N = 20$, $K = 2$ (the mean degree is thus 4) and wiring probabilities (a) $\tilde{p} = 0$ and (b) $\tilde{p} = 0.1$. The color node code is: green = household; blue = school; red = hospital; black = company.
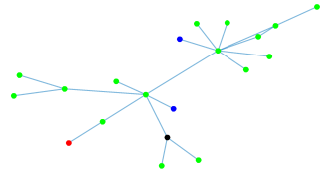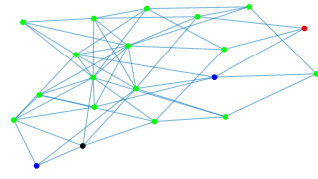
(a) $m = 1$ (b) $m = 3$

Figure 8: Scale free Barabasi Albert network with $N = 20$, $m_0 = 3$ and (a) $m = 1$, (b) $m = 3$. The color node code is: green = household; blue = school; red = hospital; black = company.
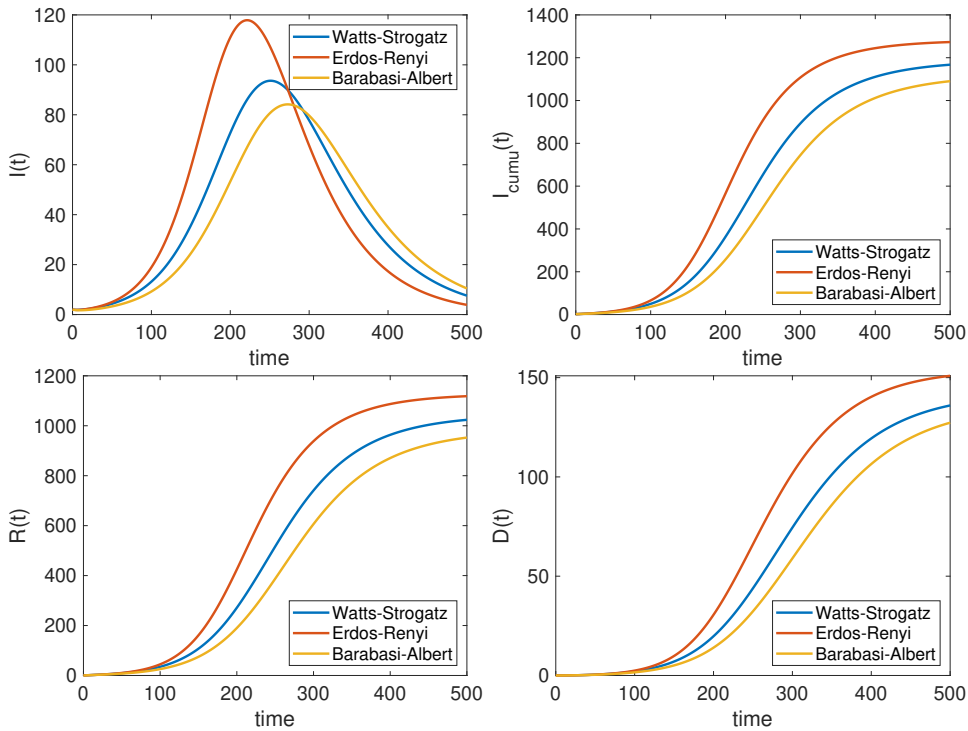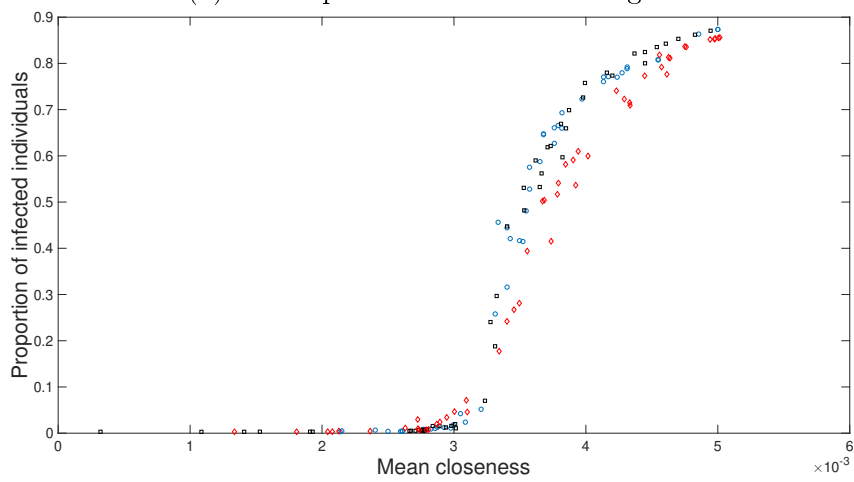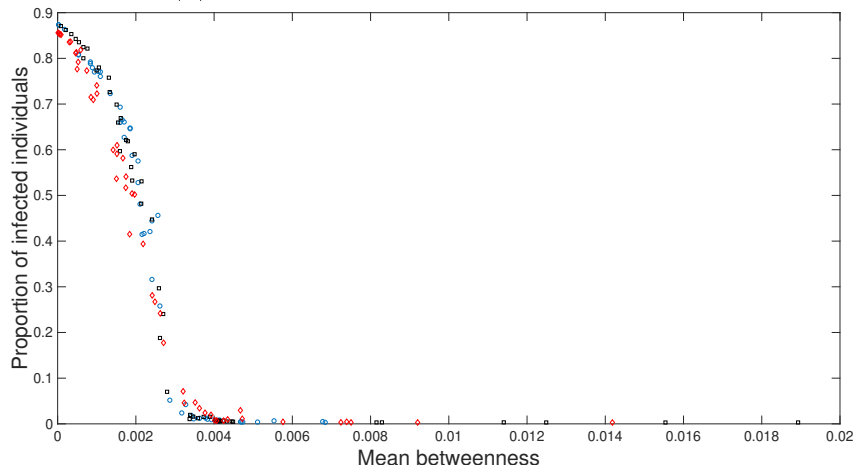

Figure 9: Infected, cumulative infected, recovered and deceased cases for three different types of networks with $N = 200$, same number of nodes of each type and of initial infected individuals: random graph with $p = 0.75$, WS with $K = 70$, $\tilde{p} = 0.1$, BA with $m_0 = m^* = 90$.

24
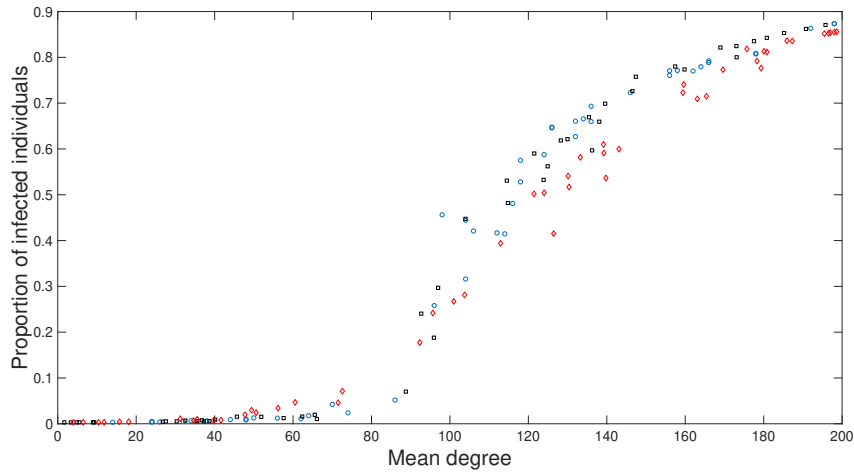
(a) Final epidemic size vs mean degree

(b) Final epidemic size vs mean closeness

(c) Final epidemic size vs mean betweenness

Figure 10: Proportion of long time cumulative infected as a function of (a) mean degree, (b) mean closeness, and (c) mean betweenness, for three different types of networks: ER (blue circles), WS (black squares), scale-free (red diamonds). Each realization generates a graph with randomly chosen parameters.
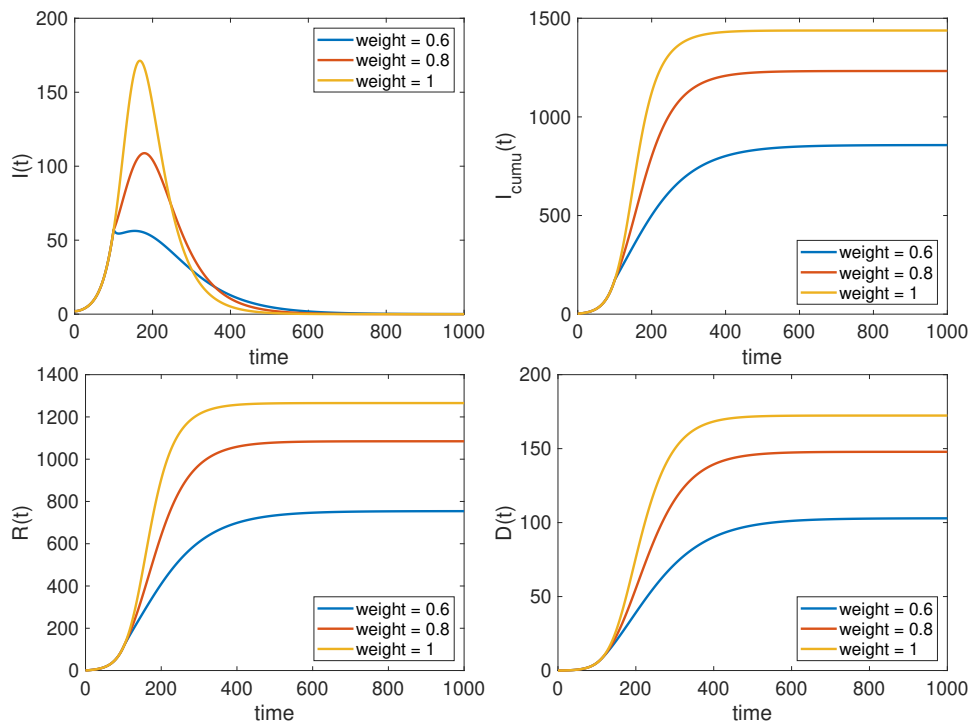
Figure 11: Infected, cumulative infected, recovered and deceased cases in a weighted Erdos-Renyi random network with $N = 200$ and $p = 0.9$. From $T_{lock} = 100$, weights are reduced to 0.8 and 0.6. The yellow curve shows the scenario without weight reduction.
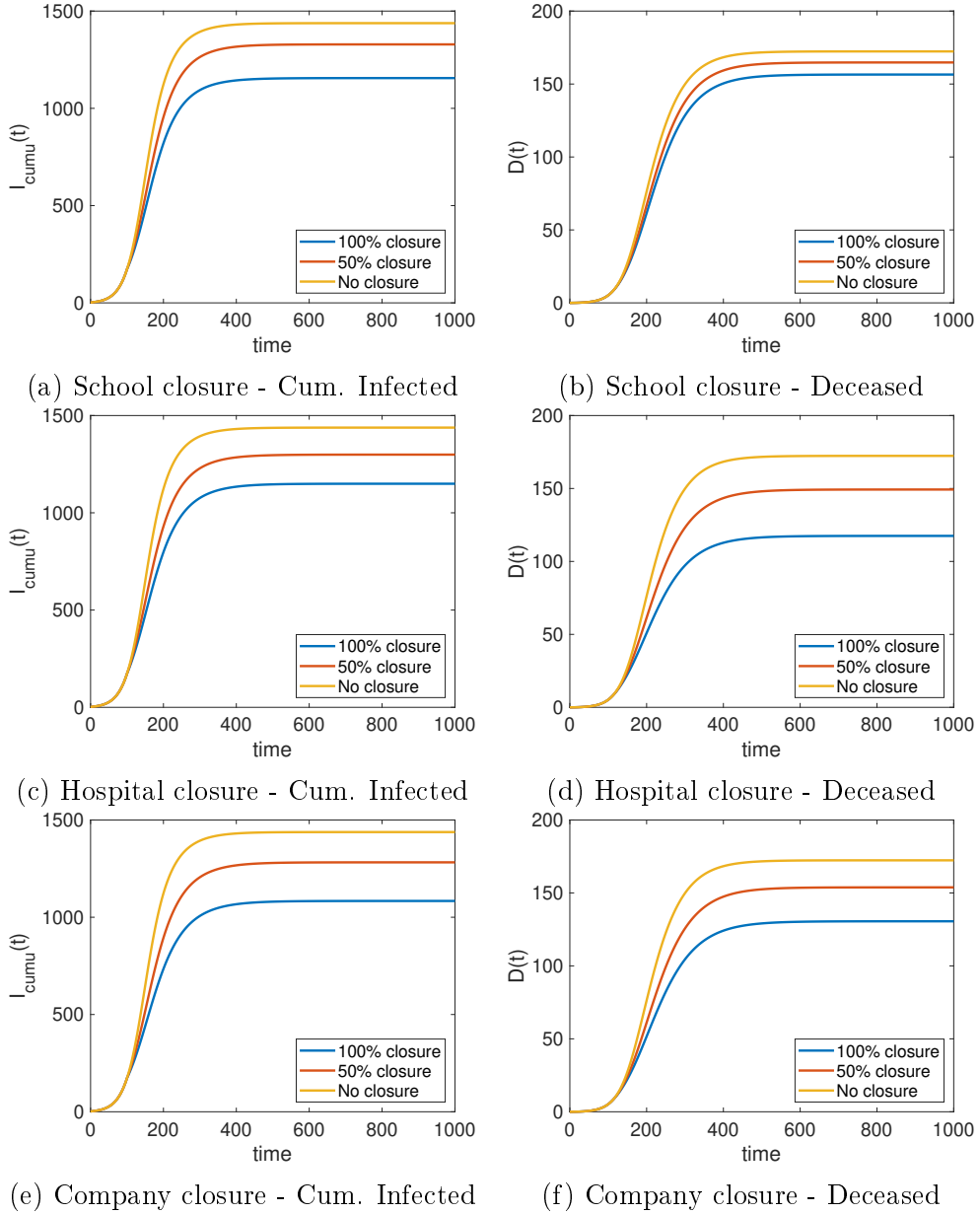
(a) School closure - Cum. Infected   (b) School closure - Deceased

(c) Hospital closure - Cum. Infected   (d) Hospital closure - Deceased

(e) Company closure - Cum. Infected   (f) Company closure - Deceased

Figure 12: Cumulative infected and deceased cases in a weighted Erdos-Renyi random network with $N = 200$ and $p = 0.9$. Scenarios showing no closure (yellow), 50% closure (red) and 100% closure (blue) of schools ((a) and (b)), hospitals ((c) and (d)), and companies ((e) and (f)), at $T_{lock} = 100$.

(a) Erdos-Renyi - Cum. Infected

(b) Erdos-Renyi - Deceased

(c) Watts-Strogatz - Cum. Infected

(d) Watts-Strogatz - Deceased

(e) Barabasi Albert - Cum. Infected
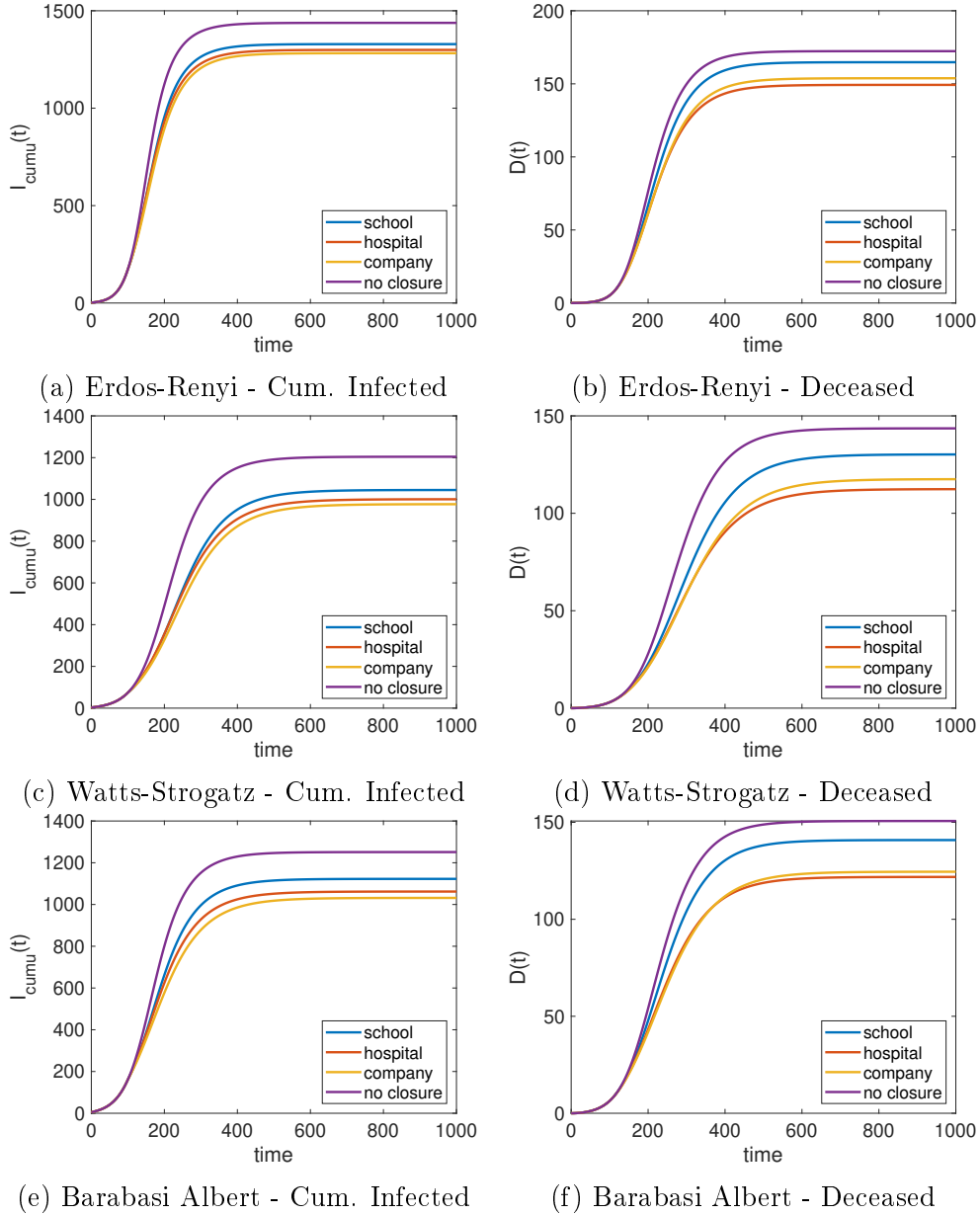
(f) Barabasi Albert - Deceased

Figure 13: Cumulative infected and deceased cases in a weighted Erdos-Renyi random network with $N = 200$ and $p = 0.9$ ((a) and (b)), small world Watts-Strogatz network with $N = 200$, $p = 0.1$ and $K = 70$ ((c) and (d)), scale-free Barabasi Albert network with $N = 200$, $m_0 = m_1 = 90$ ((e) and (f)). Scenarios show a 50% closure of schools only, hospital only and work places only at $T_{lock} = 100$, contrasted to the scenario without weight reduction.

(a) Infected   (b) Cumulative infected

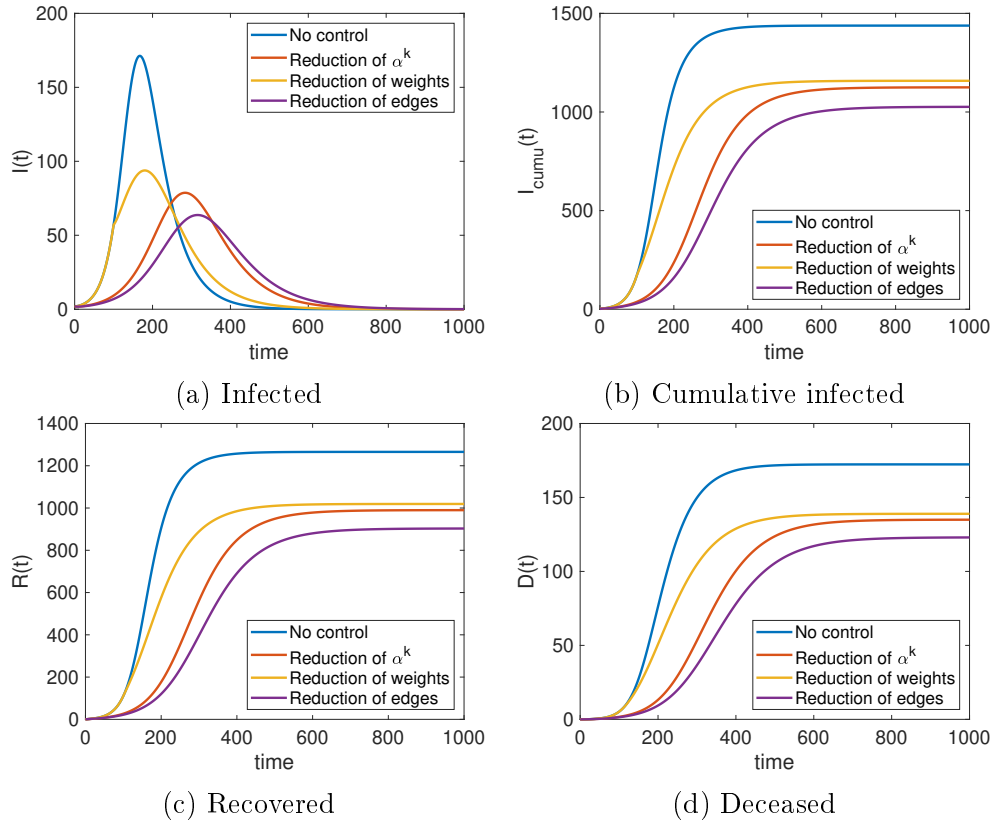(c) Recovered   (d) Deceased

Figure 14: (a) Infected, (b) cumulative infected, (c) recovered and (d) deceased cases in a weighted Erdos-Renyi random network with $N = 200$ and $p = 0.9$. At time $T_{lock} = 100$, assuming a 25% reduction for each considered scenarios: social interactions α_i^k (red), edges weights (yellow) and the total number of edges randomly reduced (purple). The scenario with no reduction is shown in blue.

(a) Infected

(b) Cumulative infected
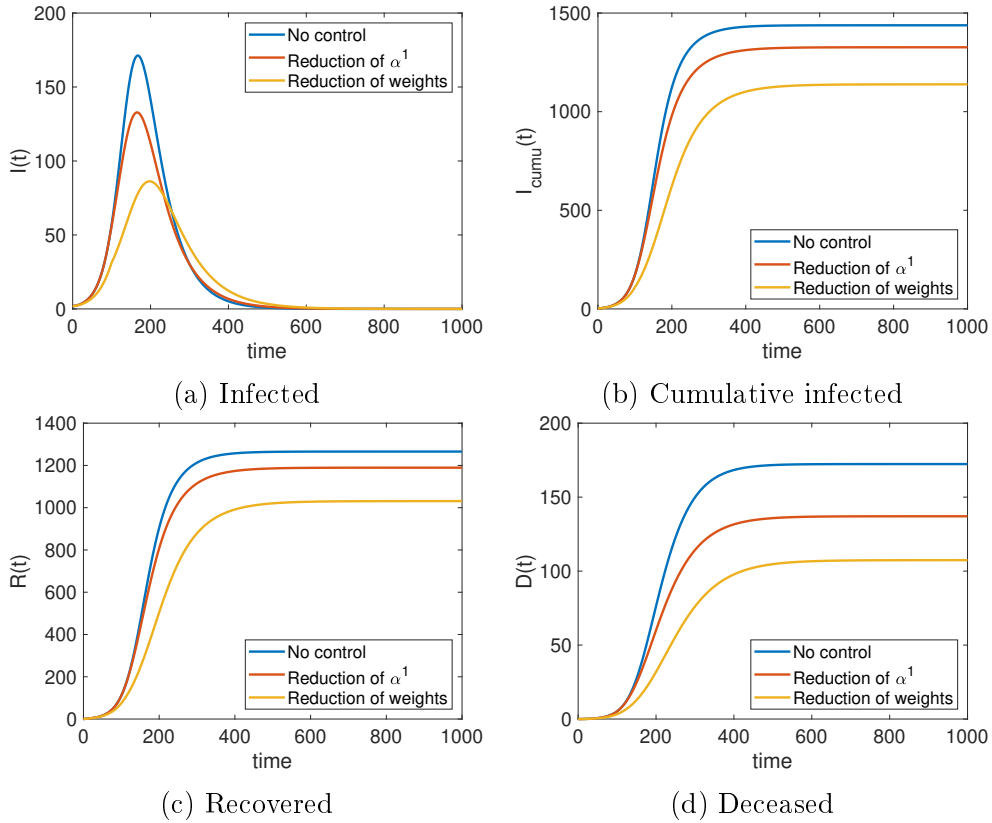
(c) Recovered

(d) Deceased

Figure 15: Protecting the vulnerable. (a) Infected, (b) cumulative infected, (c) recovered and (d) deceased cases in a weighted Erdos-Renyi random network with $N = 200$ and $p = 0.9$. At time $T_{lock} = 100$, a reduction of 50% is considered for two scenarios: social interactions involving the most vulnerable population α_1^i (red) and weight of edges connecting to hospitals (yellow). The scenario with no reduction is shown in blue.
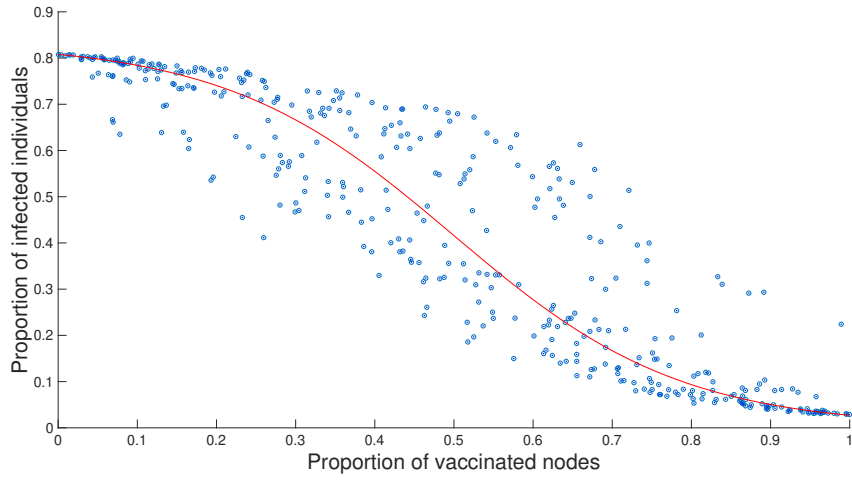
(a) Final epidemic size
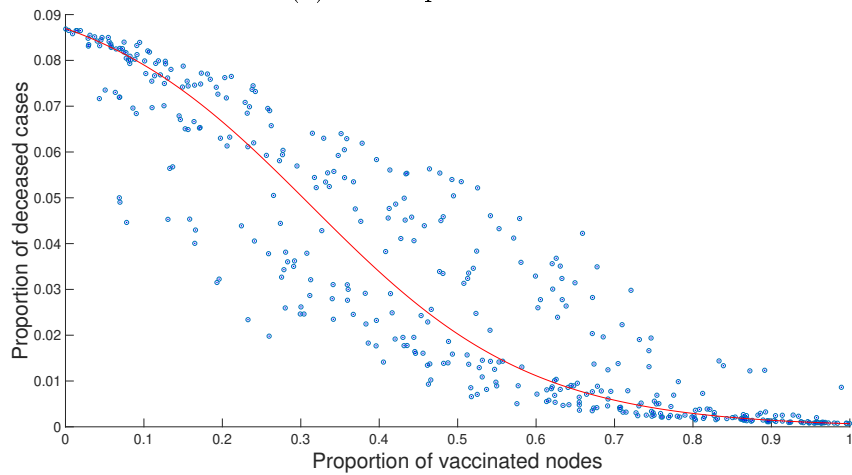
(b) Cumulative deceased cases

Figure 16: (a) Final epidemic size and (b) cumulative deceased cases vs. fraction of vaccinated nodes for 200 realizations of the experiment. Spearman correlation coefficient of -0.9 in both cases. Blue markers represent the output of each realization, and the red curve is a sigmoidal LSQ robust filter.